

Journal of Biomedical Optics

SPIEDigitalLibrary.org/jbo

Optimized off-axis cylindrical mirror- focused line-scanning system for optical coherence tomography imaging applications

Mohammad Kamal
Sivakumar Narayanswamy
Muthukumaran Packirisamy

Optimized off-axis cylindrical mirror-focused line-scanning system for optical coherence tomography imaging applications

Mohammad Kamal, Sivakumar Narayanswamy, and Muthukumar Packirisamy

Concordia University, Department of Mechanical Engineering, 1455 De Maisonneuve Boulevard West, Montreal, Quebec, H3G1M8 Canada

Abstract. The parameters of an off-axis cylindrical mirror-focused line-scanning system were studied to optimize the flatness of the 2 mm scan field. The scanning system parameters included the beam size, the distance between the scanning and the focusing mirror, the angle between the incident beam and the reflected beam, the optical scan angle, and the effective focal length of the cylindrical mirror. Because of the off-axis line-scanning system configuration, the scanning could be carried out either in the tangential (Y-scan) or in the sagittal (X-scan) plane. A 53 nm spectral bandwidth light source was used to evaluate the imaging performance of the scanning system. Since reflective optics is employed in this work for focusing, the scanning system could be used with a higher spectral bandwidth light source for optical coherence tomography applications. The effect of the angle between the incident and reflected beams, the distance between the mirrors, the focal length of the cylindrical mirror and the scanning directions, on the flatness of the scan field were studied. It was proved that the sagittal scanning is least sensitive to variations in scanning system parameters and thus provides maximum flexibility in design. © 2012 Society of Photo-Optical Instrumentation Engineers (SPIE). [DOI: 10.1117/1.JBO.17.5.056006]

Keywords: scan field flatness; line-scanning; mirror focusing; optical coherence tomography; imaging quality.

Paper 11373 received Jul. 14, 2011; revised manuscript received Feb. 29, 2012; accepted for publication Mar. 7, 2012; published online May 4, 2012.

1 Introduction

Optical coherence tomography (OCT) is a high resolution, noninvasive cross-sectional imaging technology.¹ In standard OCT systems, a single-axis or a two-axis scanner is routinely used to obtain two-dimensional (2-D) or three dimensional (3-D) imaging. A pre-objective or a post-objective lens scanning configuration is commonly utilized in OCT imaging. To perform the scanning using a pre-objective configuration, the beam is required to move away from the optical axis of the lens. Consequently, a complex lens system design is required to maximize the imaging quality throughout the scan range.² On the other hand, a simple lens system is sufficient in the case of post-objective lens configuration,²⁻⁴ but the resultant scan field is not flat. To achieve a flat scan field in the post-objective configuration, polygon scanner mirrors are commonly used.⁵ However, they are not suited for endoscopic scanning owing to their large size. Moreover, a broader spectral-band light source is required in OCT imaging for a higher axial resolution and the effective focal length (EFL) of the lenses varies as a function of the wavelengths.⁶ Consequently, the imaging quality of the lens-focused scanning system is reduced due to the chromatic aberration.⁷ In addition, the imaging quality of flying spot scanning is also reduced because of the distortion errors⁸ and motion artefacts such as eye or body motion.⁹

A line-scanning (LS) system that uses cylindrical lens-focusing has been reported for high-speed OCT imaging.¹⁰⁻¹³ In LS-OCT, a collimated beam is focused as a line on the

sample by using cylindrical optics. The line size in the focusing direction is determined by the numerical aperture (NA) of the objective lens whereas in the other direction it remains the same as that of the collimated beam. 2-D cross-sectional imaging data can be obtained by using line focused scanning with spectral-domain (SD) acquisition without requiring a mechanical scanner. On the other hand, the 3-D image data can be obtained by using line scanning with SD acquisition by integrating only a single axis scanner. As a result, line-field scanning increases the scanning speed while maintaining the sensitivity advantage of flying spot scanning with SD acquisition.¹⁰ However, the line-scanning systems developed so far, use lenses to focus the beam, thereby affecting the image quality, which is degraded by the chromatic aberration and scanning distortion errors. Mirror focusing is an alternative that can eliminate the chromatic aberration as the mirror is insensitive to the spectral bandwidth of the light source. In our earlier articles,^{14,15} a mathematical model and optical design of a cylindrical mirror-based scanning system have been reported. It was proved that, for OCT applications, the mirror focusing performs better than the lenses.

The transverse resolution depends on the NA of the scanning system and can be increased by using either a larger beam or a cylindrical mirror with a shorter EFL. In the case of endoscopic OCT imaging, the probe size prevents the use of a larger beam. Consequently, the only way to increase the transverse resolution is by using a mirror with a shorter EFL. The imaging quality of the mirror-focused scanning system does not depend on the spectral bandwidth of the light source.¹⁴ However, due to off-axis arrangement of the scanning system layout, the imaging

Address all correspondence to: Sivakumar Narayanswamy, Concordia University, Department of Mechanical Engineering, 1455 De Maisonneuve Boulevard West, Montreal, Quebec, H3G1M8, Canada. Tel: +514 848 2424, ext.7923; Fax: +514 848 3175; E-mail: nrskumar@encs.concordia.ca

quality is dependent on the geometrical arrangement of the scanning system. The scanning system parameters include the following: the incident beam size, the distance between the mirrors, the angle between the incident and reflected beams, the optical scan angle, and the EFL of the cylindrical mirror. The optimization of these parameters is required to maximize the imaging quality throughout a target scan range.

The results of a modified optical model and the experimental validation of that model are presented here. The effects of the angle between the incident and reflected beams ϕ , the distance between the mirrors d , and the EFL of the cylindrical mirror, on the flatness of the scan field were studied. In addition, scanning was performed both in the tangential (Y-scan) and in the sagittal (X-scan) planes to evaluate the effect of scanning direction on the flatness of the scan field. Two beam off-set positions from the center of the cylindrical mirror were studied to evaluate the robustness of the cylindrical mirror scanning to beam-position variations. The scan field flatness was evaluated using the Strehl ratio (SR).

2 Scanning System Configuration

Consider that, in the scanning system configuration shown in Fig. 1(a), the laser beam which is incident on a scanner mirror at N is then reflected onto a cylindrical mirror at a point C . The beam is finally focused onto the target at R . The radius of curvature (ROC) of the cylindrical mirror is r . The angle between the incident and the reflected beams is ϕ , the distance between the two mirrors is $CN = d$, and the EFL of the cylindrical mirror is $CR = f$. An optical scan angle of θ is required to scan a target scan range of L_s . The details of this model and the scanning procedure can be found in our earlier articles.¹⁴⁻¹⁶

In this system, the cylindrical mirror focuses collimated beam as a line on the target sample and the beam is required to sweep on the cylindrical mirror in order to scan the target range L_s . Because of this beam sweeping, the optical scan angle varies from $-\theta/2$ to $+\theta/2$ with respect to the angle ϕ .

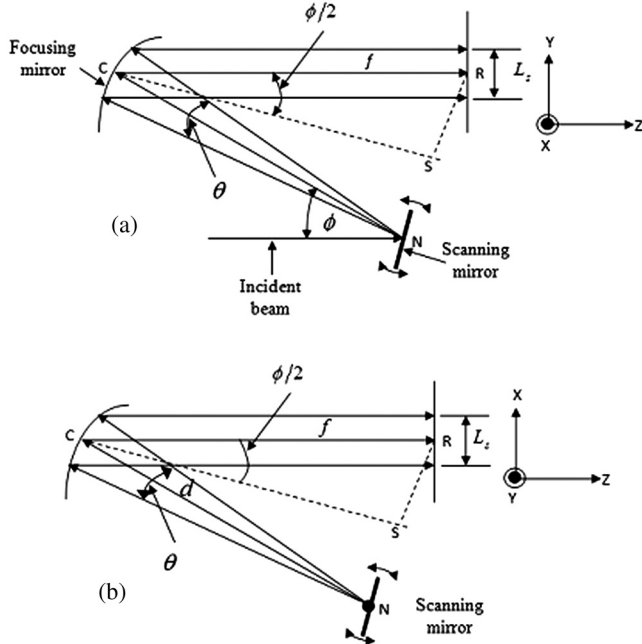


Fig. 1 Scanning system configuration (a) Y-axis scanning and (b) X-axis scanning.

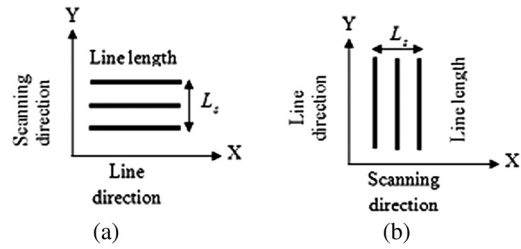


Fig. 2 2-D scan map of the (a) tangential (Y-scan) and (b) sagittal (X-scan) scanning.

For this optical scan angle, the angle between the incident and reflected beams varies from $(\phi - \theta/2)$ to $(\phi + \theta/2)$. This angular variation also depends on the distance between the mirrors and the radius of curvature of the focusing mirror. The focal length of the cylindrical mirror is half of the radius of curvature while the beam is in the optical axis of the mirror. Using an off-axis scanning system configuration, the EFL is determined by the d , θ , r , and ϕ of the configured system.¹⁵ The EFL positions also vary according to the beam position on the cylindrical mirror.

The advantage of using the cylindrical mirror is that en-face scanning requires only one directional scan. Therefore, a cylindrical mirror can be used to perform en-face scanning either in the tangential plane (Y-scan) or in the sagittal plane (X-scan) by focusing the beam in the respective direction. Y-scan and X-scan system configuration are shown in Fig. 1(a) and 1(b), respectively. In the case of X-scan, the incident beam position is perpendicular to this paper. A map of en-face scanning performed by using a Y-scan and by using an X-scan is shown in Fig. 2(a) and 2(b), respectively. If the scan direction changes from the Y-scan to the X-scan, the influence of the angle ϕ is diminished because the scanning is performed in the orthogonal direction with respect to the incident beam. As a result, the position of EFLs within the scan range varies as a function of d and θ . Hence, for a fixed d and r , the EFL positions within the scan range vary as a $f(\phi, \theta)$ in the case of tangential scanning whereas it varies as a $f(\theta)$ in the case of sagittal scanning.

3 Optical Simulation Using the Y-scan System Configuration

To evaluate the flatness of the scan field, a 2 mm beam and cylindrical mirrors with r of 51.7 and 103.4 mm were used.

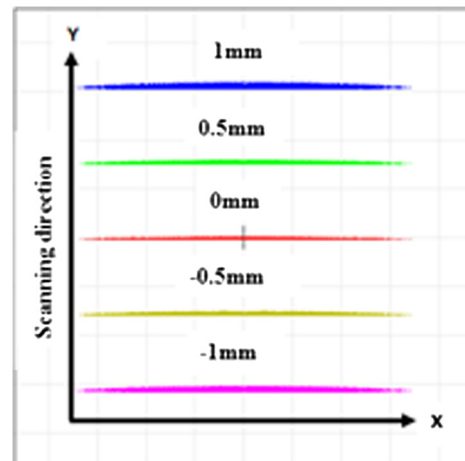


Fig. 3 Five beam positions in the 2 by 2 mm scan field.

Table 1 SR as a function of d 's for a 51.7 mm FL mirror.

d (mm)	Scan position (mm)				
	1	0.5	0	-0.5	-1
75	0.95	0.98	0.99	0.98	0.95
50	0.98	0.99	0.99	0.99	0.99
35	0.99	0.99	0.99	0.99	0.99
25	0.99	0.99	0.99	0.99	0.99
12.5	0.99	0.99	0.99	0.99	0.99

Table 2 SR as a function of d 's for a 25.85 mm FL mirror.

d (mm)	Scan position (mm)				
	1	0.5	0	-0.5	-1
75	0.22	0.45	0.93	0.42	0.23
50	0.35	0.68	0.93	0.64	0.39
35	0.6	0.85	0.93	0.8	0.64
25	0.81	0.87	0.94	0.9	0.9
12.5	0.93	0.85	0.94	0.91	0.91

Table 3 ZEMAX model parameters.

r (mm)	d (mm)	ϕ
103.4	35	30, 45, 60 deg
51.7	35	30, 45, 60 deg

Therefore, the focal length (FL) of these mirrors is 25.85 and 51.7 mm, respectively. SR¹⁴ was used for performance evaluation. An 843 nm centre wavelength light source with a spectral range of 803 to 883 nm was used in the ZEMAX model. Since mirror-focusing is insensitive to wavelength bands and it maintains zero chromatic focal shifts,¹⁴ this system can be used for any broader spectral bandwidth light source that is required for OCT imaging. The influence of the scanning system parameters

Table 5 Optimized EFLs with different ϕ .

ϕ	EFL (51.7 mm FL)	EFL (25.85 mm FL)
30 deg	49.939	24.992
45 deg	47.767	23.913
60 deg	44.778	22.43

was simulated for a 2 by 2 mm scan field by using the ZEMAX optical design software.

3.1 Effect of the Distance (d)

The effect of the distance between the scan mirror and the cylindrical mirror d was studied with the ZEMAX software for 25.85 and 51.7 mm FL mirrors with an angle ϕ of 45 deg for five different distances of d . SR was recorded at five different positions within the 2 mm scan range. In the ZEMAX model, five beam positions with an interval of 0.5 mm were defined within the 2 mm scan range. These scans at positions, indicated by -1, -0.5, 0, 0.5 and 1 mm, scan are shown in Fig. 3. The results are given in Table 1 for a 51.7 mm FL mirror and Table 2 for a 25.85 mm FL mirror. The simulation results show that, in the case of the 51.7 mm FL, almost the same SR was maintained throughout the 2 mm scan range when the distance between the mirrors d was 50 mm or lower, and if the distance was more than 50 mm, the SR drops slightly towards both ends.

In the case of the 25.85 mm FL mirror, a good SR is maintained when the mirror is located at d less than or equal to 25 mm. For a larger distance, the imaging performance drops significantly towards the ends of the scan range. Therefore, to achieve a high imaging quality, the distance between the mirrors should be equal to or less than the FL of the mirror. However, due to the experimental constraints, the distance between the mirrors d of 35 mm was used for experiments.

3.2 Effect of the Incident Angle (ϕ)

Table 3 shows the value of the parameters that were used in the ZEMAX model to evaluate the effect of the incident angle. The optical scan angle from the ZEMAX and the angular variations ($\phi \pm \theta/2$) for 51.7 and 25.85 mm FL mirrors with different ϕ are given in Table 4. Here, the optical scan or the angular variation corresponds to the 2 mm scan range for a defined ϕ .

The EFL was optimized with a different angle of ϕ for the best SR within the 2 mm scan range. The optimized EFL positions of the 51.7 and the 25.85 mm FL mirror are given in Table 5. Figure 4(a) shows the SR comparisons with these incident angles

Table 4 Angular variations simulated using the ZEMAX for a 2 mm scan range.

ϕ	Optical scan angle (θ)		Angular variation ($\phi \pm \theta/2$)	
	25.85 mm FL	51.7 mm FL	25.85 mm FL	51.7 mm FL
30 deg	4.4 deg	2.2 deg	27.8 to 32.2 deg	28.9 to 31.1 deg
45 deg	4.8 deg	2.4 deg	42.6 to 47.4 deg	43.8 to 46.2 deg
60 deg	5.2 deg	2.6 deg	57.4 to 62.6 deg	58.7 to 61.3 deg

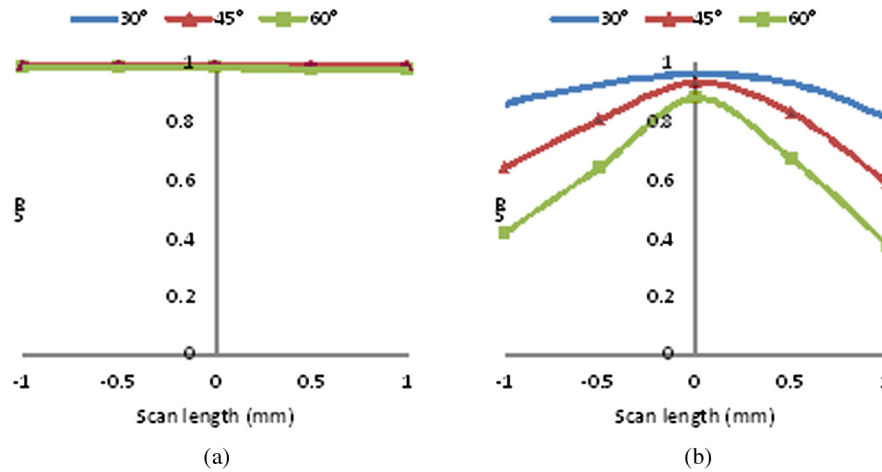


Fig. 4 SR comparisons at different incident angles using (a) a 51.7 mm FL mirror and (b) a 25.85 mm FL mirror.

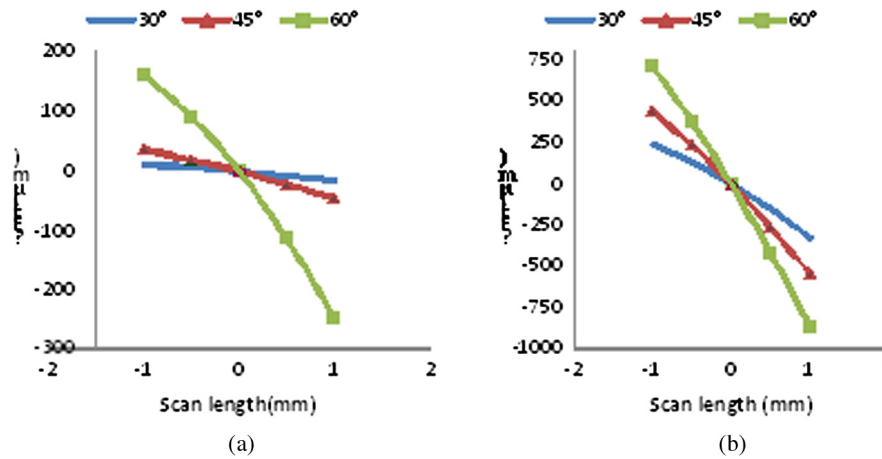


Fig. 5 EFL position variations at different incident angles with (a) a 51.7 mm FL mirror and (b) a 25.85 mm FL mirror.

for a 51.7 mm FL mirror, and Fig. 4(b) shows the SR comparisons for a 25.85 mm FL mirror at optimized EFL for the specific ϕ . In the case of the 51.7 mm FL mirror, the SR remained better than the Marechal criteria throughout the 2 mm scan range regardless of the angle ϕ . In the case of the 25.85 mm FL mirror, the SR was higher than the Marechal criteria throughout the 2 mm scan range when the incident angle was 30 deg. However, in the case of the 45 and 60 deg angles, the SR drops towards both ends of the 2 mm scan range. The SR drops because a higher optical angle is required when using a lower FL mirror to scan the same 2 mm range.

The model was optimized for a best SR for each beam position within the 2 mm scan range. The EFL position was optimized individually for five different beam positions. The EFL position variations with different incident angles for 51.7 and 25.85 mm FL mirror are shown in Fig. 5(a) and 5(b), respectively. The results show that the variation of the EFL position (Δ EFL) is higher when reducing the FL of the mirror and/or increasing the angle between the incident and reflected beams. For example in the case of the 51.7 mm FL mirror, Δ EFL is 250 μ m from the center to one end of the scan field with $\phi = 60$ deg compared to a Δ EFL of 50 μ m with $\phi = 30$ deg. Similarly at $\phi = 60$ deg the Δ EFL varies from 250 to 874 μ m if the FL of the mirror is changed from 51.7 to 25.4 mm. Because of this higher Δ EFL, the imaging quality drops significantly towards the ends of the

scan field. In order to obtain high imaging quality, the angle between the incident and reflected beams ϕ should be 0 deg making it an on-axis scanning system. Since this is not possible, flat scan field can be achieved by using an angle ϕ , which is as low as the design would permit.

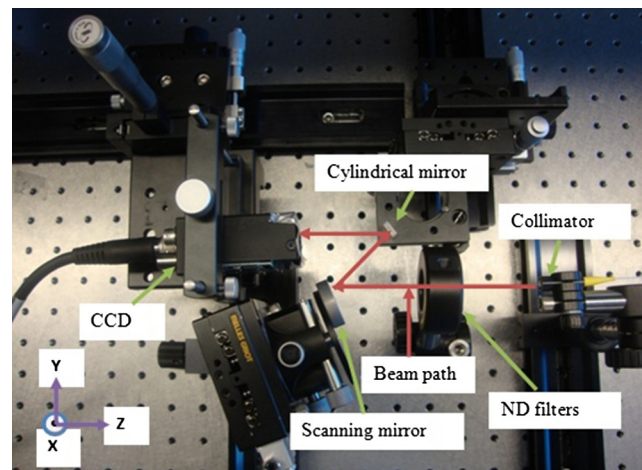


Fig. 6 Experimental setup of the scanning system.

4 Experimental Setup

The experimental setup consists of a superluminescent diode (SLD) laser, a scanning mirror, a cylindrical focusing mirror, and a CCD detector, as shown in Fig. 6. The spectral bandwidth of the SLD (Superlum HP-371) at full-width-half-maximum (FWHM) is 53 nm with a center wavelength of 843 nm. The beam was collimated by using a custom-made pigtail achromatic collimator (OZoptics) to 2 mm. The radius of curvatures of the cylindrical mirrors used for this study was 103.4 and 51.7 mm with an aperture size of 8 by 8 mm. A flat mirror mounted on a tilt and rotation stage (Newport, M-PO46N-50) was used as a scanning mirror. A 644 by 492 CCD camera (JAI CV-A11) with a pixel size of $7.4 \mu\text{m}^2$ was used to capture the beam profile. The line size at focal position depends on the size of the incident beam and the focal length of the cylindrical mirror. With a cylindrical mirror of 25.85 mm FL, the beam size ($1/e^2$) is 2 mm by $22 \mu\text{m}$ measured at 0 mm scan position. Details of the beam profile measurement and optimization have been reported in earlier publication.¹⁶

The beam reflected from the scanning mirror is blocked by the CCD camera housing before reaching on the cylindrical mirror. Hence, for the experiments, the housing was removed from the camera, enabling the use of both 51.7 and 103.7 mm r mirrors with a distance d of 35 mm. The reduction of the distance d below 35 mm or using mirrors with r less than 51.7 mm is still not possible with the CCD camera. Five line profiles that were captured for performance evaluation within the 2 mm scan range are at -1 , -0.5 , 0 , 0.5 , and 1 mm. The

captured beam profiles were analyzed using a program written using LabVIEW software.

5 Result and Discussion

Consistency of the imaging quality throughout the target scan range is required to maintain the flatness of the scan field. Y-scans and X-scans were performed by rotating the scanning mirror in the respective direction for a target scan range of 2 mm. SR was used to evaluate the flatness of the scanning system with 51.7 and 25.85 mm FL mirrors. Spread function was used to obtain the SR from the ZEMAX model as well as from the experimental measurements.

5.1 Flatness Evaluation With Y-Scan System Configuration

In the Y-scan configuration, the collimated beam was focused in the Y-axis while the X-axis remained the same as the collimated beam size. The system parameters that were discussed in Sec. 3 were used for the experiments. The scanning was performed by rotating the scanning mirror in the Y-axis. Five beam profiles were captured with an interval of 0.5 mm within the 2 mm scan range. The experiments were repeated for the incident angles of 30, 45, and 60 deg with a distance of $d = 35$ mm. Comparisons of SR between ZEMAX modeling and the experiments for a 51.7 mm FL mirror, with the beam positions set at incident angles of 30, 45, and 60 deg are shown in Fig. 7(a) to 7(c), respectively. In the case of 30 and 45 deg incident angles, the SR remained above the Marechal

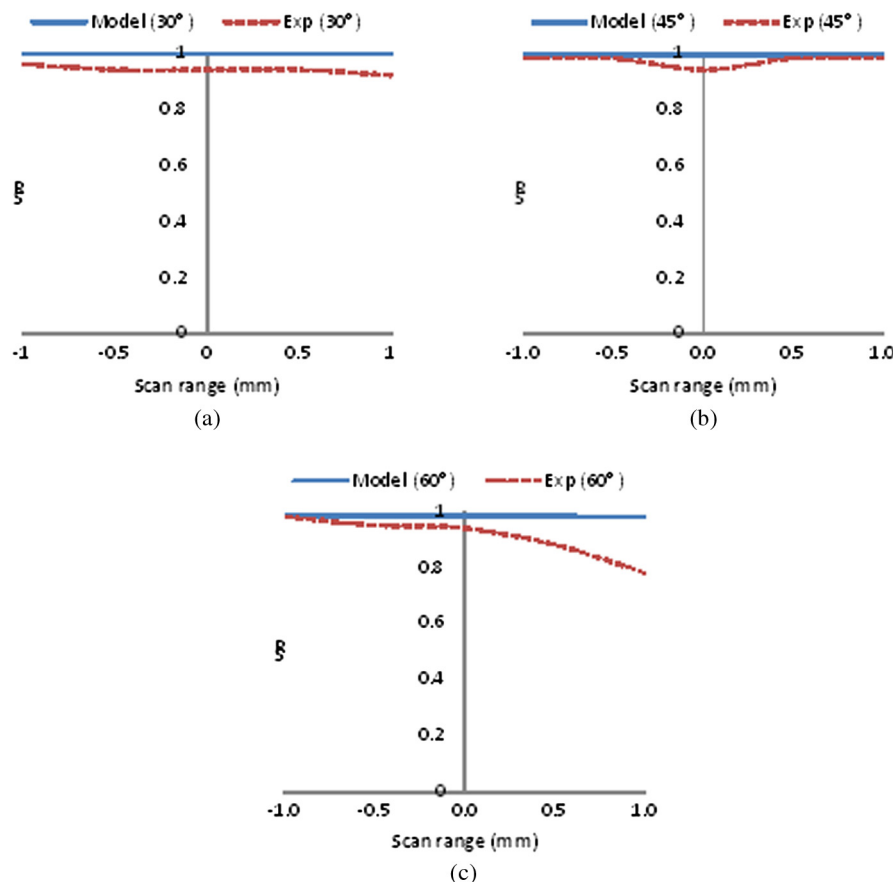


Fig. 7 SR comparison of 51.7 mm FL mirror with the angle of (a) $\phi = 30$ deg (b) $\phi = 45$ deg, and (c) $\phi = 60$ deg.

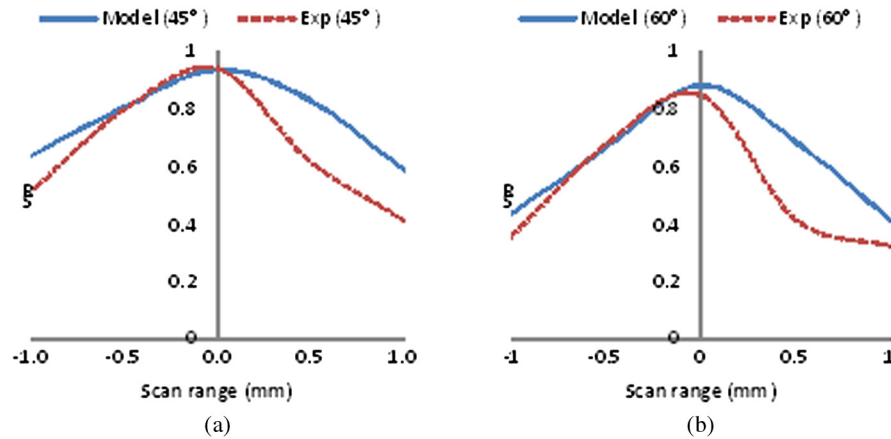


Fig. 8 SR comparison for 25.85 mm FL mirror with the angle of (a) $\phi = 45$ deg and (b) $\phi = 60$ deg.

criteria throughout the 2 mm scan range. In the case of the 60 deg incident angle, the SR is 2.5% lower than the Marechal criteria at one end of the 2 mm scan range.

Because of the off-axis configuration, the beam is blocked by the camera housing for $\phi < 45$ deg with a 25.85 mm FL. Thus, the experiments were restricted to $\phi < 45$ deg and $\phi < 60$ deg with a 25.85 mm FL. In the case of shorter FL mirrors, a larger optical scan angle was required to scan the 2 mm scan range compared to that of the longer FL mirrors, resulting in increased EFL position variations. The model results and the experimental results with 45 and 60 deg angles are shown in Fig. 8(a) and 8(b), respectively. In the case of 45 deg angle, the variation between model and experimental measurements is 29% whereas this variation is 39% in the case of 60 deg angle. However, with the different incident angle the result shows the same trend within the scan range. The modeling results in Sec. 3 show that the scanning system maintained a consistent SR within the 2 mm scans range with an angle of $\phi = 30$ deg. Therefore, variations of the imaging quality can be reduced by using a lower angle of ϕ , as discussed in Sec. 3.2.

The experiments were performed in a free space optics system, where the system geometric parameters such as the distance d , the angle ϕ and the r , were restricted by the size of the optics and that of the CCD camera. However, in the real imaging system, scanning would be performed on the sample instead of on the CCD camera, and the scanning mirror can be replaced by a

MEMS mirror. Design of a miniature scanning system was reported in our earlier work.¹⁵ The mirror distance of $d = 10$ mm and the angle of $\theta = 20$ deg with the 14.95 mm FL mirror were used in the miniature scanning system simulation. With these parameters, the scanning system maintained an SR more than 0.97 throughout the 2 mm scan range. Therefore, the developed scanning can be used in endoscopic OCT imaging as well as in external OCT imaging applications with a higher transverse resolution.

5.2 Flatness Evaluation with X-Scan System Configuration

X-scanning was performed to evaluate the effect of the scanning direction on the flatness of the scan field. The ZEMAX optical design software does not permit changing the scanning as well as the focusing direction for this off-axis scanning system configuration. Thus, the flatness of the scan field was experimentally evaluated by using an X-scan. For this set of experiments, same system parameters that were used in the optical model and in the Y-scan configuration were repeated. X-scans were performed by changing the focusing and the scanning direction from the Y-axis to the X-axis. When the scanning direction was changed from Y to X, the scanning was performed in the orthogonal plane with respect to the incident beam. Because of that the incident angle ϕ does not have any influence on the

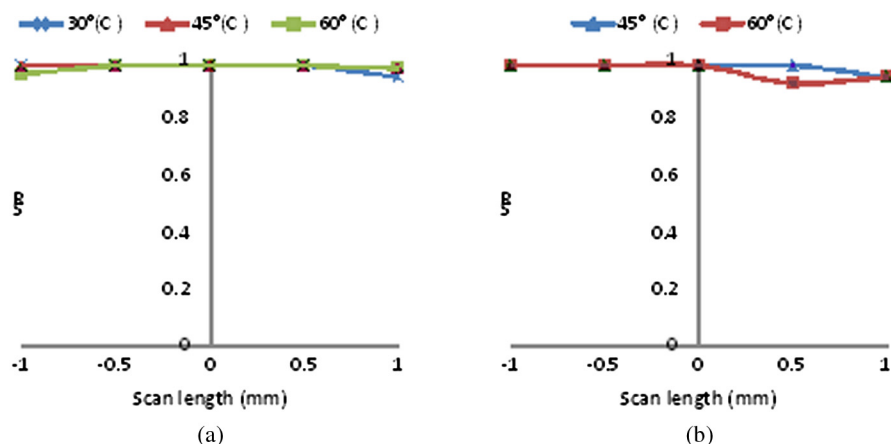


Fig. 9 X-scan SR comparison with the beam position at C for (a) 51.7 mm, and (b) 25.85 mm FL mirror.

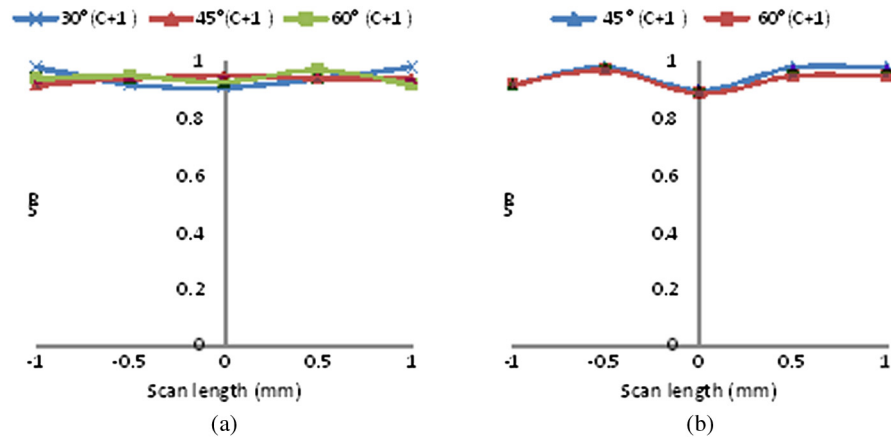


Fig. 10 X-scan SR comparison with the beam position at C + 1 for (a) a 51.7 mm FL mirror and (b) 25.85 mm FL mirror.

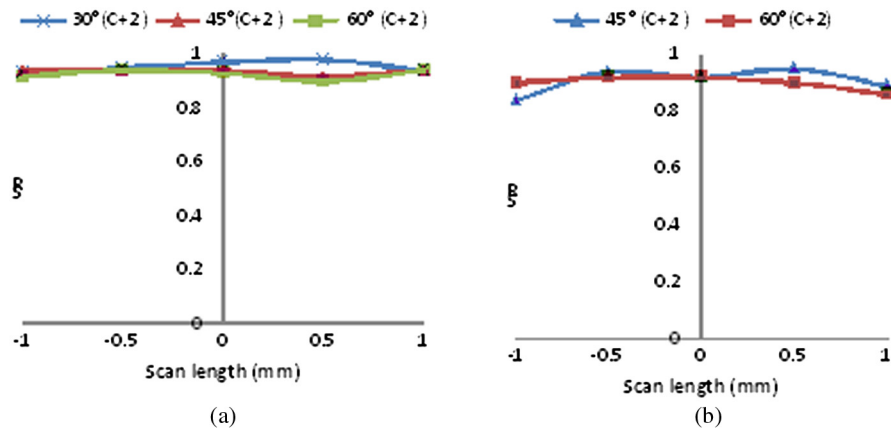


Fig. 11 X-scan SR comparison with the beam position at C + 2 for (a) 51.7 mm FL mirror and (b) 25.85 mm FL mirror.

angular variations during the scanning. Hence, the EFL positions vary as a function of the scan angle. The incident angles of 30, 45 and 60 deg were used with the 51.7 mm FL mirror. Because of the experimental constraints, in the case of the 25.85 mm FL mirror, the experiments were limited to the incident angles of 45 and 60 deg. Experiments were performed by positioning the beam at the center C of the mirrors. Five beam profiles were captured within the 2 mm scan range, and then the profiles were processed to extract the SR value.

Comparisons of the SR for the beam position at C are shown in Fig. 9(a) and 9(b) for the 51.7 mm FL mirror and for the 25.85 mm FL mirror, respectively. The experimental results show that the SR maintained above the Marechal criteria of 0.8 throughout the 2 mm scan range regardless of the focal length and the incident angle.

Two off-set positions on the cylindrical mirrors were used to evaluate the sensitivity of the scanning system to variations in beam positioning. For both mirrors, a 1 mm off-set from the

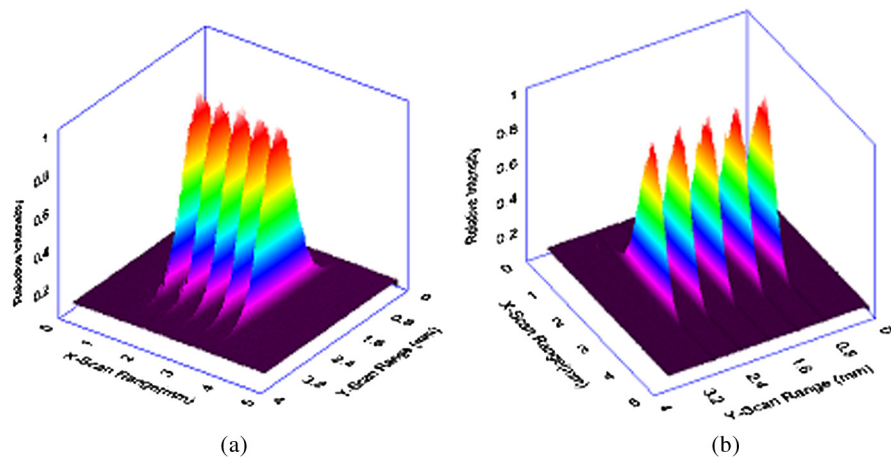


Fig. 12 3-D map of 51.7 mm FL mirror with $\phi = 60$ deg (a) Y-scan and (b) X-scan configuration.

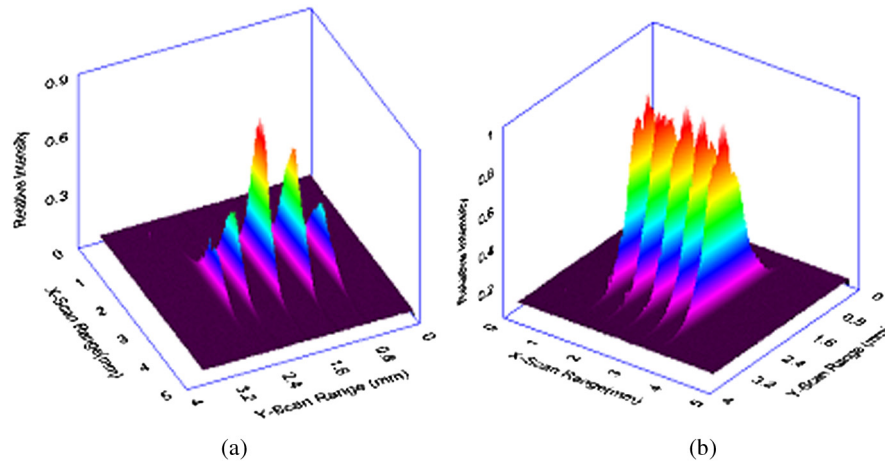


Fig. 13 3-D map of 25.85 mm FL mirror with $\phi = 60$ deg (a) Y-scan and (b) X-scan configuration.

center ($C + 1$) and a 2 mm off-set from the center ($C + 2$) were studied. Five beam profiles were recorded within the 2 mm scan range for each off-set position. The SR comparisons for these beam positions are shown in Figs. 10 and 11, respectively. Experimental results show that the SR maintained above the Marechal criterion throughout the 2 mm scan range regardless of the beam position, the incident angle, and the radius of curvatures. Therefore, the developed scanning system provides flat scan field by maintaining consistent SRs throughout the 2 mm scan range.

3-D beam profiles from the Y-scan and from the X-scan made by using a 51.7 mm FL mirror and a 25.85 mm FL mirror are shown in Figs. 12 and 13, respectively. In the case of the 51.7 mm FL mirror, the beam profiles show consistency throughout the 2 mm scan range in both scanning directions. In the case of the 25.85 mm FL mirror, the beam profile lost consistency towards the ends of the 2 mm scan range when using the Y-scan system configuration. The reason for this loss is attributed to the higher angular variation with respect to the angle between the incident and the reflected beam for

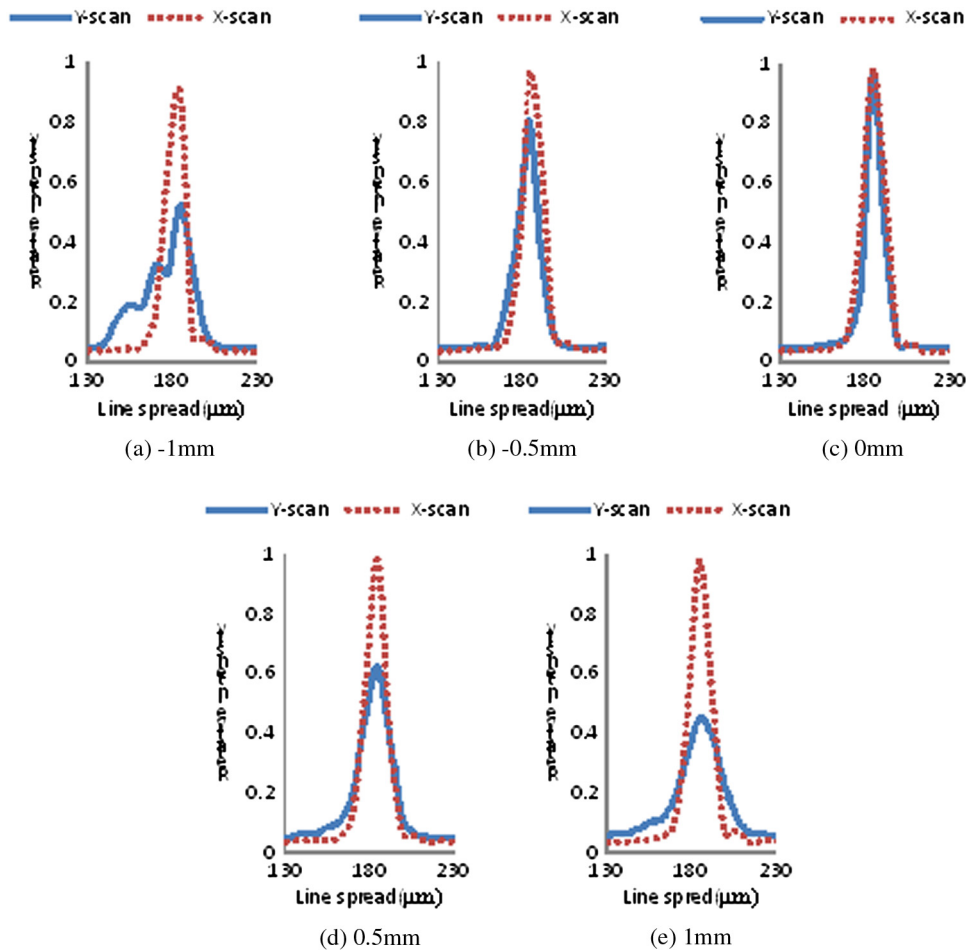


Fig. 14 X-scan and Y-scan transverse resolution within 2 mm scan range at different scan position.

the same scan field of 2 mm. In the case of the X-scan system configuration, the beam profiles maintained consistency throughout the 2 mm scan range. In this configuration, the scanning was performed in the orthogonal plane with respect to the incident beam. Therefore, the incident angle does not have any impact on the angular variation.

5.3 Transverse Resolution Comparison

The shape and the size of the spread function determine the transverse resolution. Imaging quality depends on the consistency of the transverse resolution throughout the scan range. Transverse resolution in the line focusing direction is quantified by using FWHM of the spread function. Therefore, a consistent FWHM is required to achieve a flat scan field image. To evaluate the effect of the scan direction on the FWHM, the spread function was extracted from five beam profiles. Figure 14 shows the spread function at five scan positions within a 2 mm scan range using the 25.85 mm FL mirror at the angle $\phi = 45$ deg. In the case of the X-scan, a $15 \mu\text{m}$ transverse resolution is maintained throughout the 2 mm scan range. In the case of the Y-scan, a $15 \mu\text{m}$ transverse resolution was achieved only at the center of the scan field. It drops significantly towards the ends of the scan field.

6 Conclusion

A robust line-scanning system has been demonstrated by using cylindrical mirror focusing. A 53 nm spectral bandwidth light source with a centre wavelength of 843 nm was used in the developed scanning system. A 25.85 mm focal-length cylindrical mirror and a 51.7 mm focal-length cylindrical mirror were used to focus a 2 mm collimated beam. The effect of the angle between the incident beam and the reflected beam and the distance between the mirrors was studied. The flatness of the scan field was demonstrated by using tangential scanning. For high-performance imaging with the developed system, the geometric parameters of the scanning system, such as the angle between the incident beam and the reflected beam should be as low as the design would permit and the distance between the mirrors should be smaller than or equal to the focal length of the cylindrical mirror. The improvement of the imaging performance by using sagittal scanning

was demonstrated and proved that sagittal scanning provides robust performance regardless of the scanning system parameters and beam off-set.

References

1. D. Huang et al., "Optical coherence tomography," *Science* **254**(5035), 1178–1181 (1991).
2. Leo Beiser, *Unified Optical Scanning Technology*, Wiley, New Jersey (2003).
3. H. Ra et al., "Three-dimensional in vivo imaging by a handheld dual-axes confocal microscope," *Opt. Express* **16**(10), 7224–7232 (2008).
4. C. E. Webb and J. D. C. Jones, *Handbook of Laser Technology and Applications*, Institute of Physics Publishing, Bristol and Philadelphia (2004).
5. Leo Beiser, *Laser Scanning Notebook*, SPIE Press, The International Society for Optical Engineering, Bellingham, Wash. (1992).
6. Eugene Hecht, *Optics*, Addison-Wesley, San Francisco (2002).
7. W. Drexler, "Ultrahigh-resolution optical coherence tomography," *J. Biomed. Opt.* **9**(1), 47–74 (2004).
8. M. Chen, Y. Chen, and W. Hsiao, "Correction of field distortion of laser marking systems using surface compensation function," *Optic. Laser. Eng.* **47**(1), 84–89 (2009).
9. S. H. Yun et al., "Motion artifacts in optical coherence tomography with frequency-domain ranging," *Opt. Express* **12**(13), 2977–2998 (2004).
10. Y. Nakamura et al., "High-speed three-dimensional human retinal imaging by line-field spectral domain optical coherence tomography," *Opt. Express* **15**(12), 7103–7116 (2007).
11. Sang-Won Lee and Beop-Min Kim, "Line-field optical coherence tomography using frequency-sweeping source," *IEEE J. Sel. Top. Quant. Electron.* **14**(1), 50–55 (2008).
12. B. Grajciar et al., "Parallel Fourier domain optical coherence tomography for in vivo measurement of the human eye," *Opt. Express* **13**(4), 1131–1137 (2005).
13. T. Endo et al., "Profilometry with line-field Fourier-domain interferometry," *Opt. Express* **13**(3), 695–701 (2005).
14. M. Kamal, S. Narayanswamy, and M. Packirisamy, "Optical design of a line-focused forward-viewing scanner for optical coherence tomography," *Appl. Opt.* **49**(31), 6170–6178 (2010).
15. M. Kamal, N. Sivakumar, and M. Packirisamy, "Optical modeling of a line-scan optical coherence tomography system for high-speed three-dimensional endoscopic imaging" *Proc. SPIE* **7386**, 738607 (2009).
16. M. Kamal, N. Sivakumar, and M. Packirisamy, "An off-axis cylindrical mirror focused line scanning system with high imaging quality for broad spectral band," *J. Opt.* **13**(10), 105502 (2011).